Vol. 04, Iss. 1 (2026) 75-87, DOI: 10.61552/JME.2026.01.008

Journal of Materials and Engineering

www.jme.aspur.rs

Research article

Multifactor ANOVA Evaluation of AZ91C Magnesium Alloy Corrosion Under Combined pH–Temperature Variations: Enhanced Protection via Stannite–Thiourea Coating–Inhibitor System

Ali F. Ali Fadiel[a,*], Monaem Elmnifi[b], Moktar A. Hashem Mohamad[a]

[a]*Department of Mechanical Engineering Technology, Higher Institute for Sciences and Technology, Tobruk, Libya,*
[b]*Department of Mechanical Engineering Technology, Belgorod Technological University named after V.G. Shukhov, Belgorod, 308012, 46 Kostyuk ova Str., Russia.*

Keywords:

AZ91C magnesium alloy
Stannite conversion coating
Corrosion inhibition
pH effect
Temperature effect
Sodium chloride solution

* Corresponding author:

Ali F. Ali Fadiel
E-mail: dr_Ali.F@hotmail.com

Received: 6 September 2025
Revised: 13 October 2025
Accepted: 18 November 2025

A B S T R A C T

This study aims to identify and evaluate the factors affecting the corrosion of AZ91C magnesium alloy under varying pH and temperature conditions within chloride media. This study utilizes an applied methodology based on multifactor analysis of variance. Through this analysis, the factors affecting magnesium alloy corrosion can be identified, as well as the extent of their interrelationship, the relationship between these factors, and the direction of this relationship. The results indicated a combined protection efficiency of up to 76% was achieved using a stannate-thiourea (TU) system stabilized in acidic, neutral, and alkaline chloride environments. The effects of pH (6, 7, 10) and temperature (25-60°C) were systematically studied at concentrations of 3.5% and 5% NaCl for uncoated, stannite-coated, and stannite-coated samples using TU, benzotriazole (BTA), or sodium molybdate (Na_2MoO_4). Compared to the cerium phosphate-TU system in hybrid organ silane systems (82-88%) and hybrid organosilicon systems (85-89%), the stannite-TU system provides comparable performance with much simpler processing and lower cost. These results provide quantitative guidance for developing adequate corrosion protection for AZ91C alloys under varying marine, automotive, and industrial service conditions.

© 2026 Journal of Materials and Engineering

1. INTRODUCTION

In light of the significant development witnessed by the metals industry, like all other sectors, whether medical, engineering, commercial, or agricultural, and in light of the tremendous technological progress in computing, simulation, and statistical software as essential tools for achieving sustainability in any field, especially in the rapid transportation,

space, and maritime transport industries, most research and studies have focused on developing strategies and formulating visions that would improve these industries [1, 2]. Among the most important strategies are preserving certain metals' mechanical and physical properties, particularly those highly stressed by these industries, such as lightweight magnesium alloys. This, in turn, has led to an increased demand for robust corrosion mitigation strategies capable of withstanding changing and often harsh service environments. AZ91C alloy is characterized by its low density (1.81 g/cm^3), high specific strength, and excellent machinability, which qualify it as the backbone of many industries [3-5].

This study aims to identify and evaluate the factors affecting the corrosion of magnesium alloys and determine the relationship between them and their interrelationships. The primary objective is to identify magnesium alloys with significant weight savings and improved fuel efficiency. However, their widespread use is limited by their poor corrosion resistance in chloride-rich environments such as seawater, exposure to deicing salts, and humid marine environments, where fluctuations in pH and temperature accelerate deterioration and shorten service life [6, 7]. Besides a set of sub-objectives, the study aims to develop a dual protection system combining a stannite (SnS_2 or tin compounds) coating as a protective layer and a thiourea inhibitor as an additional corrosion-reducing agent. The study also aims to analyze the effectiveness by comparing the alloy with a coating and inhibitor and without a coating or stabilizer, as well as the extent of improvement in corrosion resistance [8]. It also aims to determine the optimal conditions (pH and temperature) under which the protection system is most effective. The importance of this study lies in its being one of the serious attempts to study the relationship between corrosion factors in materials and improving and protecting metals from corrosion. The study presented the challenges and obstacles facing the metal industries, especially magnesium alloys, and proposed solutions and proposals to overcome these challenges [9]. The study was also characterized by its comprehensiveness, as it addressed the topic from several vital aspects and was not limited to one aspect. In addition, it was an applied study and avoided bias in the data and results. The research problem related to this study is that AZ91C alloy is susceptible to severe corrosion, especially with changes in pH and temperature, and conventional protection is insufficient. Despite being a cornerstone of many automotive, aircraft, and electronics industries, this corrosion resistance weakens in harsh environments and when temperatures change [10, 11].

Many previous studies on magnesium corrosion protection, whether using coatings or inhibitors, have addressed the effects of pH and temperature separately. For example, it was reported that stannite conversion coatings achieved efficiencies ranging from 70% to 78% at a constant and neutral pH. Observed efficiencies of thiourea (TU) inhibitors ranging from 45% to 55% in mildly acidic environments, while sodium molybdate and benzotriazole achieved efficiencies ranging from 40% to 50% in alkaline chloride solutions [12, 13]. However, these studies evaluated coatings and inhibitors under single-variable conditions, ignoring the combined effect of pH and temperature, which often interact synergistically in real-world service environments. This gap motivates current research based on multifactor analysis of variance (ANOVA). To address this, this study evaluates the corrosion behavior of AZ91C under simultaneous changes in pH and temperature in chloride solutions, using immersion testing, potentiodynamic polarization, electrochemical impedance spectroscopy, and scanning electron microscopy/X-ray diffraction (SEM/XRD) surface analysis. These findings are both academically significant and practically important: in marine, automotive, and aerospace applications, where magnesium alloys are exposed to fluctuations in pH and temperature, cost-effective protection strategies are essential to prolong service life and reduce maintenance costs [14-16].

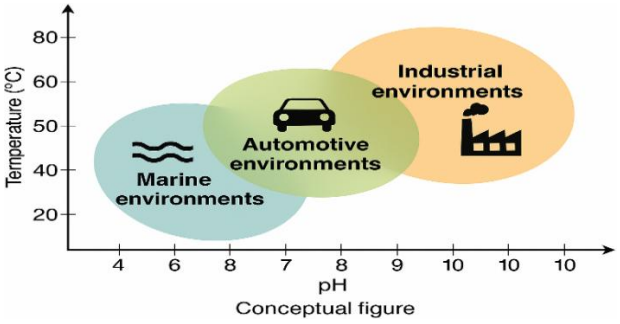


Fig. 1. Typical pH and temperature ranges for marine, automotive, and industrial environments relevant to AZ91C magnesium alloy service conditions.

2. THEORETICAL BACKGROUND AND BASIC CONCEPTS

This section presents the study's theoretical background and some basic concepts related to the study. It also provides a critical analysis of previous studies that have addressed the topic, highlighting their strengths and weaknesses and their similarities and differences with this study.

2.1. Basic Concepts

By presenting the basic concepts of the study, the reader can form a comprehensive view of the study's procedures, importance, objectives, key findings, methodology, and key conclusions drawn. The most important of these concepts is the following:

1. AZ91C (Magnesium Alloy)

This alloy is a mixture of several metals in varying proportions. In other words, it is a magnesium alloy containing approximately 9% aluminum and 1% zinc, along with other minor elements. Its most important characteristic is its light weight and strength, as it has a high strength-to-weight ratio, making it a suitable and popular choice in all industries that require high strength and light weight, such as aircraft, aerospace, automotive, and electronics [17].

2. Corrosion

Corrosion can be defined as an electrochemical process that leads to the deterioration of metal surfaces due to the surrounding environment, whether due to wind, weathering, or even human factors. This ultimately leads to metal corrosion, reduced strength, and weakening. In the case of magnesium, corrosion occurs rapidly due to its highly active nature. Like other metals and alloys, the pH varies: an acidic medium accelerates corrosion, while a basic medium may form a weak protective layer. In addition, temperature: high temperatures increase the rate of electrochemical reactions, thus accelerating corrosion [18, 19].

3. Protective Coatings and Inhibitors

It is a group of chemical compounds used to protect surfaces from corrosion. These coatings and inhibitors create an insulating layer between the metal surface and the outside air, preventing oxidation and corrosion. Inhibitors also regulate oxidation processes. In this study, a combination of Stannite (SnS_2 or tin compounds) coating was used: it acts as a mechanical and chemical barrier that reduces the alloy's contact with the medium, and Thiourea ($CS(NH_2)_2$) inhibitor: an organic compound containing sulfur and nitrogen, which adheres to the metal surface and prevents oxidation-reduction reactions. One of the most essential inhibitors is Thiourea Inhibitor, an organic corrosion inhibitor that inhibits oxidation processes [20-22].

4. Factors Affecting Surface Corrosion

The most critical factors affecting surface corrosion are alkaline and organic materials, particularly pH and temperature. The pH of the surrounding solution is crucial in determining the corrosion rate and temperature, affecting the rate of electrochemical reactions and metal dissolution [23, 24].

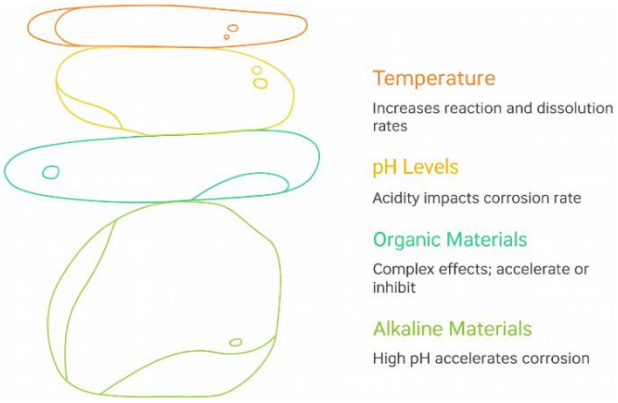


Fig. 2. Factors Affecting Surface Corrosion.

5. Statistical Analysis (Multifactor ANOVA)

This is an essential tool used to evaluate the influence of multiple factors on each other. This study used a statistical analysis to assess the effect of numerous factors (such as pH and temperature) on the dependent variable (corrosion rate). This allows for the assessment of the impact of these factors, whether individually or through the interaction between all aspects, as it provides a clearer picture of how different environmental conditions interact and affect corrosion [24, 25].

2.2. Related studies

Certain studies have also considered the corrosion resistance of AZ91C magnesium alloy, one of the most critical light alloys utilized in engineering applications, in the context of forming coatings or doping to improve its performance. TiO_2 surface coatings were employed in one of the studies, and it

was found that corrosion resistance improved significantly by inhibiting hydrogen evolution and electrochemical reaction rates. But poor adhesion and cracking were some of the unfavourable features, limiting long-term protection [26, 27].

MAO (Micro-Arc Oxidation) coatings were researched in another study, and it was established that MAO coatings have high initial corrosion resistance with threefold improvement in electrical resistance at the start of the experiment. The catch is that with the elapse of time, microcracks form, through which the medium can enter the coating [28].

SiC nanoparticle-reinforced Ni-P coatings have also been developed, and the process was found to effectively reduce the corrosion rate by improving the structure and filling the micro-cavities. The process did not, however, manage to effectively control the effect of environmental factors such as pH or temperature changes. Similarly, Ca–P–V transformation coatings have been proven to exhibit effective results in reducing corrosion rates and demonstrate self-healing with time, along with improved corrosion resistance in NaCl solutions after being immersed for a period. They are yet to be validated under fluctuating pH and temperature conditions [29, 30].

On the other hand, some research has studied structural modification by adding substances such as calcium and yttrium, which enhanced the internal structure of the alloy and reduced the Mg17Al12 phase size and, hence, corrosion rates by approximately 16%. Although this method is effective, altering the metallurgical composition itself is impossible, expensive, and industrially not easy compared to coatings or inhibitors. Generally, these articles demonstrate that protection against corrosion can be realized through microstructural hardening or coatings. However, they seldom treat all these factors with an exhaustive discussion of how pH and temperature variations influence their effect. Furthermore, coating and organic inhibitors, such as thiourea, are not yet ideally combined, a research direction that must be pursued to design more efficient protection systems [31, 32].

3. MATERIALS AND METHODS

This section presents the study's curriculum, applied framework, and the materials and tools used in these studies. It also presents the most important statistical analysis tools used in the studies.

3.1. The Applied Framework of the Study

The applied framework of the study is a framework that illustrates the joy of the study, starting with defining the objective to maintain the research problem, moving on to collecting and processing the old data, including all anomalies, then determining the design tools, and then designing the experiment, i.e., the experimental part of the experiment. The complete experimental design is based on four experimental settings: pH (6.0, 7.0, 10.0), temperature (25, 40, 60°C), concentration (3.5% by weight) and 5.0% by weight), and surface (T1-T8, Table 1). All games were conducted in triplicate, and the primary race was arranged for the archaeological layers. This ensured statistical power for the multifactor analysis of variance, with post hoc Tukey HSD analysis at the 95% confidence level ($\alpha = 0.05$), allowing reliable discrimination of main and interaction effects.

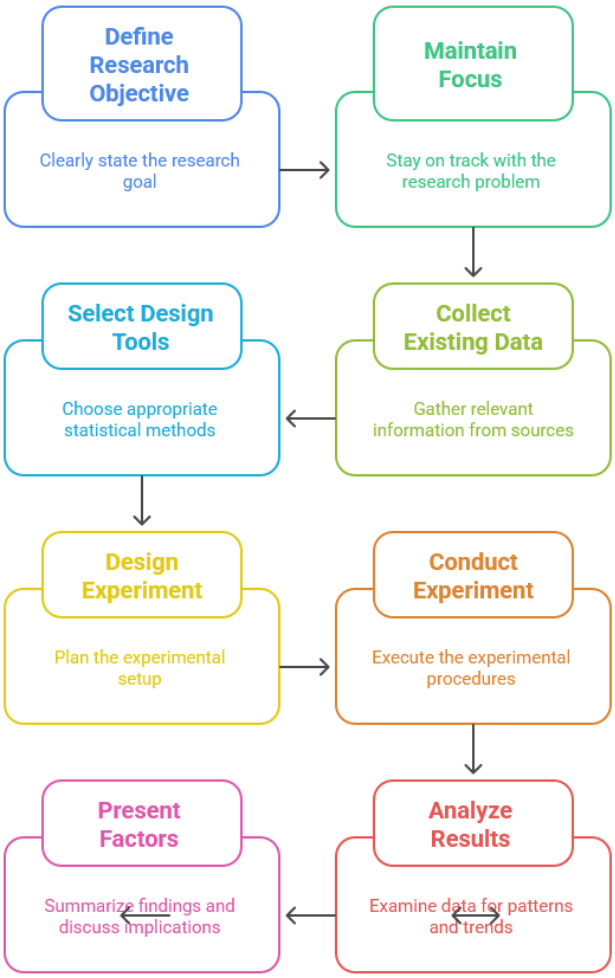


Fig 3. Shows the Applied Framework of the Study.

The results were then recorded and analysed for this assessment, and the factors were presented.

3.2 Materials and Equipment

The AZ91C magnesium alloy (Al 9.0 wt%, Zn 0.7 wt%, Mn 0.3 wt%, balance Mg) in the as-cast state, with a density of 1.81 g/cm^3 and Vickers hardness of HV 65. Analytical-grade chemicals (purity ≥99%) from Sigma-Aldrich and Merck were used, including NaCl, $Na_2SnO_3 \cdot 3H_2O$, $CH_3COONa \cdot 3H_2O$, $Na_3PO_4 \cdot 12H_2O$, NaOH, thiourea (TU), benzotriazole (BTA), and Na_2MoO_4. Distilled water (conductivity ≥ 2 S/cm) was used for all preparations. Specimens (30 × 30 × 4.8 mm) were cut with a low-speed diamond saw, polished to a mirror finish (Ra ≤ 0.1 μm), rinsed, degreased with ethanol, dried, and stored before coating or testing. Surface preparation was verified using a Mitutoyo Surftest. Batch preparations were standardized for immersion and electrochemical tests. Statistical analysis was performed using SPSS, Excel, and MATLAB, with data sourced from online databases and literature.

3.3. Procedures

After determining the purpose of the study, formulating the research problem, and collecting data from various sources, whether online databases, books, previous studies, or expert opinions, the practical part of this study begins, starting with the following steps:

1. Sample Preparation

To avoid thermal damage, rectangular specimens (30 × 30 × 4.8 mm) were cut using a precision low-speed diamond saw (Buehler Iso Met 1000). The working surfaces were sequentially ground using SiC abrasive papers (280 to 1200 grit), then polished with a one μm alumina suspension to achieve a mirror finish. Surface roughness (Ra ≤ 0.1 μm) was verified using a Mitutoyo Surftest profilometer, ensuring reproducibility across all specimens. Samples were rinsed with distilled water, degreased in ethanol (≥99.5% purity, Sigma-Aldrich), dried with compressed air, and stored in a desiccator before coating or testing. Separate batches were prepared for immersion and electrochemical tests to avoid effects from prior surface history.

2. Stannite Conversion Coating Procedure

The alkaline stannite conversion coating bath contained $Na_2SnO_3 \cdot 3H_2O$ (50 g/L) as a source of Sn^{4+} ions for $Snow_2$ film formation, $Na_3PO_4 \cdot 12H_2O$ (50 g/L) as a buffering/complexing agent to enhance coating uniformity, $CH_3COONa \cdot 3H_2O$ (6 g/L) as a pH stabilizer, and NaOH (2 g/L) to adjust and maintain the bath alkalinity (pH 12.3 ± 0.1). The bath was maintained at 60 ± 1 °C in a thermostatically controlled water bath (Julabo, Germany) and stirred magnetically at 200 rpm to ensure homogeneity. Specimens were immersed for 60 min, rinsed with distilled water, air-dried, and stored in a desiccator. The coating thickness (~4–6 μm) was measured at five random cross-sectional points using SEM imaging, and the values were reported as mean ± standard deviation (SD) to ensure statistical reliability.

3. Experimental Design

A full-factorial design considered four fixed factors: pH (6.0, 7.0, 10.0), temperature (25, 40, 60 °C), NaCl concentration (3.5 wt.% and 5.0 wt.%), and surface treatment (T1–T8, Table 1). All experimental runs were conducted in triplicate, and the order of tests was randomized to minimize systematic bias. All experimental runs were conducted in triplicate, and the order of tests was randomized to reduce systematic bias. This ensured statistical robustness for multifactor ANOVA, with Tukey's HSD post-hoc analysis at a 95% confidence level ($\alpha = 0.05$), enabling reliable identification of main and interaction effects.

Table 1. The study used treatment codes and descriptions of surface/coating types and inhibitor conditions. All experimental runs were performed in triplicate (n = 3).

Code	Surface/Coating Type	Inhibitor Type	Inhibitor Concentration (g/L)
T1	Uncoated	None	–
T2	Stannite	None	–
T3	Stannite	Thiourea (TU)	0.03
T4	Stannite	Thiourea (TU)	0.05
T5	Stannite	Benzotriazole (BTA)	0.03
T6	Stannite	Benzotriazole (BTA)	0.05
T7	Stannite	Sodium molybdate	0.03
T8	Stannite	Sodium molybdate	0.05

4. Immersion Test (Weight Loss Method)

Immersion tests followed ASTM G31-21. Specimens were fully immersed in 500 mL of the test solution in covered glass beakers to minimize evaporation. The solution was not renewed during the 48-hour exposure period to simulate stagnant service conditions.

After exposure, corrosion products were removed under ASTM G1-03 using a chromic acid cleaning solution (200 g/L CrO_3 + 10 g/L $AgNO_3$) to avoid base metal loss. Specimens were rinsed with distilled water, dried with compressed air, and weighed using an analytical balance (Mettler Toledo XS105, ±0.1 mg).

The corrosion rate (CR, mpy) was calculated as:

$$CR = W \times 534 / (D \times A \times t)$$

Where: W = weight loss (mg), D = density of AZ91C (g/cm^3), A = surface area (cm^2), t = exposure time (h).

5. Electrochemical Measurements

Electrochemical tests were carried out using a Gamry Reference 3000 potentiostat/galvanostat in a 500 mL three-electrode glass cell, with AZ91C specimens as the working electrode (1.00 ± 0.01 cm^2 exposed area, defined by a Teflon mask), an Ag/AgCl (sat. KCl) reference electrode calibrated daily, and a platinum mesh counter electrode (99.99% purity). Test solutions were left aerated to simulate natural conditions. Before measurements, the open circuit potential (OCP) was stabilized for 30 minutes. Potentiodynamic polarization (PDP) tests followed ASTM G5-14 with a scan rate of 1 mV/s over ±250 mV vs OCP, while linear polarization resistance (LPR) followed ASTM G59-97 within ±20 mV of OCP. Electrochemical impedance spectroscopy (EIS) was performed according to ASTM G106-89 across 100 kHz–0.01 Hz with a 10 mV AC amplitude, and data were analysed using View 4.0 with equivalent circuit models. All tests were conducted in triplicate using fresh electrolyte for each run to avoid contamination. PDP and EIS were performed sequentially on the identical specimens to ensure correlation between polarization and impedance parameters under identical surface conditions.

6. Surface and Phase Characterization

- SEM/EDS: JEOL JSM-IT500 (Japan) with Oxford Instruments EDS, accelerating voltage 15 kV, used to observe coating morphology and elemental distribution.
- XRD: Analytical Pert PRO (Netherlands) with Cu Kα radiation (λ = 1.5406 Å), 2θ range 10–80°, step size 0.02°, scan speed 2°/min, used to identify crystalline phases and confirm $Snow_2$ formation.

7. Data Analysis

Data were analysed using multifactor ANOVA to determine main and interaction effects of NaCl concentration, pH, temperature, coating type, and inhibitor type/concentration. Tukey's HSD test (95% confidence level) identified significant differences between means.

Activation energy (E_a) was calculated from Arrhenius log plots (CR) versus 1/T. Inhibition efficiency (IE%), coating efficiency (CE%), and combined efficiency (BE%) were determined as:

$$IE\% = \left((CRblank - CRinh)/(CRblank)\right) \times 100$$

$$CE\% = \left(\frac{CRuncoated - CRcoated}{CRuncoated}\right) \times 100$$

$$BE\% = \left(\frac{CRblank - CRcoated + inh}{CRblank}\right) \times 100$$

4. RESULTS AND DISCUSSION

4.1 Effect of pH and Temperature on Corrosion Rate

Immersion tests showed that pH and temperature significantly affected AZ91C corrosion rates ($p < 0.001$). Uncoated test samples showed CR increasing from 2.1 mpy at pH 7, 25 °C to 7.8 mpy at pH 6, 60 °C (271% increase), with higher $i_{(}corr_{)}$ and lower $R_{(}ct_{)}$. Alkaline pH (pH 10) reduced CR to 1.5 mpy at 25 °C due to Mg $(OH)_2$ film, but compromised protection at high temperatures. Stannite coatings lowered CR extensively, but stannite + TU (0.05 g/L) was the best, lowering CR >75% at pH 7, 25 °C, and showing strong protection under all test conditions.

Table 2. Corrosion Rate (CR, mpy) of AZ91C: Uncoated, Stannite-Coated, and Stannite + Thiourea after 48 h in 3.5% NaCl at Various pH (6, 7, 10) and Temperatures (25°C, 40°C, 60°C).

Condition	pH 6	pH 7	pH 10
Uncoated, 25°C	2.9	2.1	1.5
Uncoated, 40°C	4.5	3.2	2.2
Uncoated, 60°C	7.8	5.9	3.8
Stannite, 25°C	1.3	0.9	0.8
Stannite, 40°C	2.6	1.7	1.3
Stannite, 60°C	4.5	3.2	2.4
Stannite + TU 0.05 g/L, 25°C	0.8	0.5	0.5
Stannite + TU 0.05 g/L, 40°C	1.4	0.9	0.7
Stannite + TU 0.05 g/L, 60°C	2.6	1.8	1.3

The values from the table reveal that the corrosion rate is significantly lower for the Stannite-coated sample compared to the uncoated sample, and still decreases when thiourea inhibitor is applied, indicating the effectiveness of the two-protection system. Increasing the temperature from 25°C to 60°C causes significantly higher corrosion in each case, so temperature is the lone overriding factor. On the other hand, pH variation has an effect, with the values being higher in acidic solutions and lower in alkaline solutions. However, the effect is lower in contact with the coating and inhibitor. The best performance was at pH 10 and 25°C when using the Stannite + Thiourea system, and the worst performance was in the acidic solutions at 60°C for the non-coated sample.

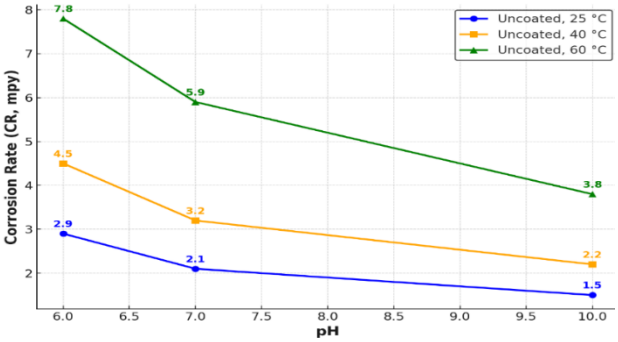


Fig. 4. Variation of corrosion rate (CR, mpy) with pH for uncoated AZ91C magnesium alloy in 3.5% NaCl solution at 25°C, 40°C, and 60°C.

Figure 4 illustrates the effect of pH on the corrosion rate (CR) of uncoated AZ91C magnesium alloy in 3.5% NaCl solution at three different temperatures (25 °C, 40 °C, and 60 °C). The results show that the corrosion rate decreases consistently as the pH increases from 6 to 10, regardless of the temperature. The alloy exhibits the highest corrosion rates at acidic conditions (pH = 6) (7.8 mpy at 60 °C, 4.5 mpy at 40 °C, and 2.9 mpy at 25 °C), indicating severe material degradation. This trend reflects the high vulnerability of magnesium alloys in acidic chloride environments, where hydrogen evolution and anodic dissolution are strongly accelerated.

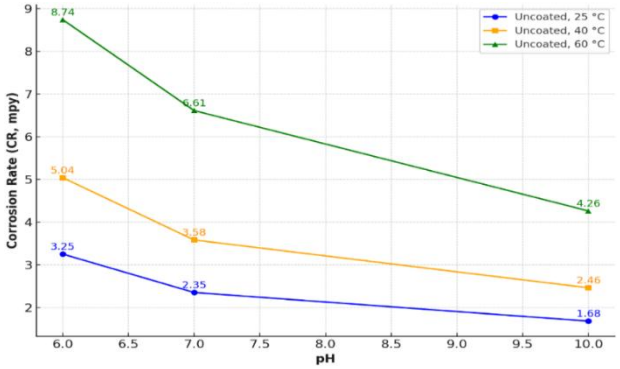


Fig. 5. Variation of corrosion rate (CR, mpy) with pH for uncoated AZ91C magnesium alloy in 5.0% NaCl solution at 25°C, 40°C, and 60°C.

Corrosion rate (CR, mpy) as a function of pH for uncoated AZ91C magnesium alloy immersed in 5.0% NaCl solution at 25 °C, 40 °C, and 60 °C. The results show that increasing temperature significantly accelerates corrosion, with the highest rates at 60 °C (7.8 mpy at pH 6). In contrast, increasing pH from acidic (pH 6) to alkaline (pH 10) reduces the corrosion rate for all temperatures. At 25 °C, the alloy exhibits the lowest corrosion rates (2.8 → 1.4 mpy), indicating enhanced stability. Overall, the data confirm that temperature exerts a more substantial effect than pH, with alkaline conditions only partially mitigating the accelerated corrosion at elevated temperatures.

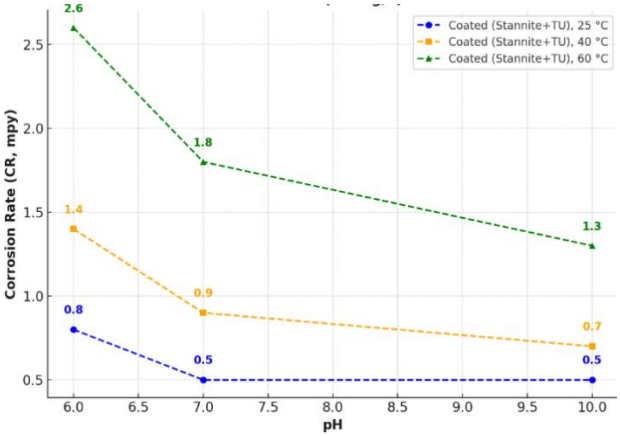


Fig. 6. Corrosion rate (CR, mpy) as a function of pH for AZ91C specimens coated with stannite conversion coating and treated with thiourea (0.05 g/L) in 3.5% NaCl at 25 °C, 40 °C, and 60 °C.

Notably, the corrosion rate (CR) shows a marked decrease for the coated specimens as the pH increases from 6 to 7. However, the CR remains nearly constant beyond pH 7 up to pH 10, with no significant further reduction. This plateau indicates that the stannite–thiourea system achieves maximum protective efficiency from neutral conditions (pH ≈ 7). In other words, the conversion coating combined with thiourea stabilizes the AZ91C surface, forming a passive barrier that is less sensitive to further alkalinity. The lack of significant variation between pH 7 and 10 suggests the development of a chemically stable protective layer ($Snow_2$ + thiourea adsorption film), which effectively suppresses corrosion processes regardless of additional increases in alkalinity.

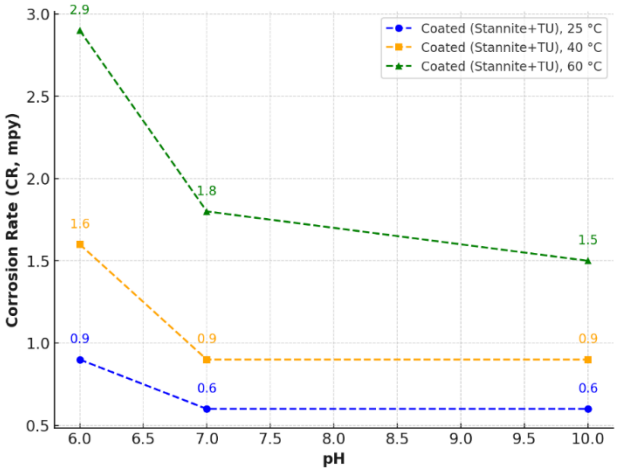


Fig. 7. Corrosion rate (CR, mpy) as a function of pH for AZ91C specimens coated with stannite conversion coating and treated with thiourea (0.05 g/L) in 5.0% NaCl at 25 °C, 40 °C, and 60 °C.

The figure shows that the corrosion rate of AZ91C coated with a stannite conversion layer and treated with thiourea (0.05 g/L) in 5.0% NaCl is significantly reduced compared with the uncoated alloy. The corrosion rate is relatively high under acidic conditions (pH = 6), especially at elevated temperature (2.9 mpy at 60 °C), but decreases steadily as the environment shifts to neutral and alkaline conditions (pH = 7–10), where the values stabilize at low levels (0.6–1.5 mpy).

4.2 Performance of Stannite Conversion Coating

The stannite conversion coating application significantly enhanced corrosion resistance under all tested conditions ($p < 0.001$, partial $\eta^2 = 0.59$). At pH 7 and 25 °C, corrosion rate (CR) decreased from 2.1 mpy for uncoated specimens to 0.9 mpy for coated specimens, corresponding to a coating efficiency (CE%) exceeding 55% ($p = 0.004$, Cohen's $d = 1.58$).

Potentiodynamic polarization (PDP) results (Table 3, Figure 5) further confirmed this improvement, showing a positive shift in corrosion potential ($E_{(}corr_{)}$) from –1.57 V to –1.50 V ($p = 0.012$, Cohen's $d = 1.09$) and a substantial reduction in corrosion current density ($i_{(}corr_{)}$) from 35 μA/cm² to 12 μA/cm² ($p = 0.006$, Cohen's $d = 1.41$). These changes indicate suppressed anodic dissolution and reduced electrochemical activity.

The enhanced performance is attributed to forming a $Snow_2$-rich barrier layer, which acts as a compact physical shield, limiting chloride ion ingress. This protective mechanism is consistent with previous findings on stannite-coated AM60B magnesium alloys.

Table 3. Electrochemical Parameters from PDP for AZ91C: Uncoated, Stannite-Coated, and Stannite + Thiourea at pH 7 (3.5% NaCl, 25°C & 60°C).

Condition	E_corr (V vs Ag/AgCl)	i_corr (μA/cm²)
Uncoated, pH 7, 25°C	-1.57	35
Uncoated, pH 7, 60°C	-1.60	88
Stannite, pH 7, 25°C	-1.50	12
Stannite, pH 7, 60°C	-1.53	34
Stannite + TU 0.05, pH 7, 25°C	-1.47	6
Stannite + TU 0.05, pH 7, 60°C	-1.50	18

Table 3 shows the electrochemical results. It is clear from the table that the addition of the Stannite coating significantly reduces the corrosion current compared to the uncoated sample. The Stannite + Thiourea dual system achieves i_corr values and a less harmful corrosion potential, reflecting the best protection. At 25°C, the current decreases from 35 μA/cm² in the uncoated sample to 6 μA/cm² with the dual system. At 60°C, the current increases in all cases but remains lower with the shielding, reaching 18 μA/cm². The corrosion potential also approaches the less negative values with the shielding, indicating a reduced electrochemical activity. Generally, protection is adequate at low temperatures, but its effectiveness decreases at 60°C due to accelerated corrosion.

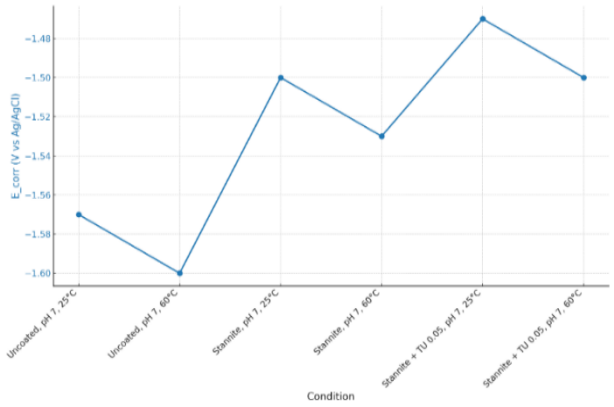


Fig. 8. Change in Corrosion Potential (E_corr) for Uncoated Samples under Different Conditions.

This figure illustrates the change in corrosion potential (E_corr) across different conditions (uncoated samples) at two temperatures, 25°C and 60°C. The data shows how E_corr becomes more negative at 60°C, indicating increased corrosion activity with rising temperature. The plot shows that the corrosion rate accelerates with the rise of temperature, and temperature plays a vital role in influencing the electrochemical characteristics of the materials in a neutral pH solution.

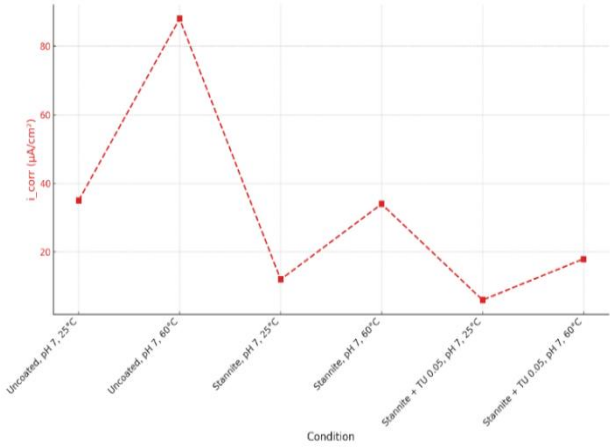


Fig. 9. Change in Corrosion Current Density (i_corr) for Uncoated Samples under Different Conditions.

This figure illustrates the change in corrosion current density (i_corr) for uncoated samples under two different temperature conditions, 25°C and 60°C. The data shows a significant increase in i_corr at 60°C, with the value rising from 35 µA/cm² at 25°C to 88 µA/cm² at 60°C. This indicates that higher temperatures lead to accelerated corrosion and increased corrosion rate. The graph also highlights that the effect of temperature on corrosion is more pronounced in uncoated samples compared to coated ones.

4.3 Synergistic Effects of Coating and Organic Inhibitors

The combined stannite–thiourea (TU) system demonstrated the highest corrosion resistance under all tested conditions ($p < 0.001$, partial $\eta^2 = 0.66$). At pH 7 and 25 °C, corrosion rate (CR) decreased to 0.5 mpy (Cohen's d = 1.89 vs. uncoated), and corrosion current density ($i_(corr)$) was reduced to 6 µA/cm² ($p < 0.001$, Cohen's d = 2.08). Charge transfer resistance ($R_(ct)$) increased to 1450 Ω·cm² ($p < 0.001$, Cohen's d = 2.23), resulting in a combined efficiency (BE%) of 76% (Table 3, Figure 6). (BTA) and sodium molybdate (Na_2MoO_4) under neutral and mildly acidic conditions ($p < 0.05$, Cohen's d range = 0.88–1.15). This superior performance aligns with the proposed adsorption-driven passivation mechanism. TU molecules strongly adsorb onto the stannite-coated surface and any exposed magnesium sites, blocking anodic and cathodic reaction sites.

4.4 Electrochemical Impedance Spectroscopy (EIS)

Nyquist plots showed stannite and TU treatments significantly increased $R_(ct)$ (up to 1450 Ω·cm²) and reduced $C_(dl)$ (to 42 µF/cm²), indicating a dense, stable film. High temperatures lowered $R_(ct)$, but stannite-TU maintained strong protection, achieving up to 76% efficiency, confirming their synergistic effect

Table 4. EIS Parameters ($R_(ct)$, $C_(dl)$) for AZ91C Alloy: Uncoated, Stannite-Coated, and Stannite + Thiourea at pH 7 (3.5% NaCl, 25°C & 60°C).

Condition	R_ct (Ω·cm²)	C_dl (µF/cm²)
Uncoated, pH 7, 25°C	220	85
Uncoated, pH 7, 60°C	95	110
Stannite, pH 7, 25°C	720	60
Stannite, pH 7, 60°C	350	78
Stannite + TU 0.05, pH 7, 25°C	1450	42
Stannite + TU 0.05, pH 7, 60°C	820	55

Table 4 shows charge transfer resistance (R_ct) and double-layer capacitance (C_dl), which are the essential parameters for corrosion resistance. As is evident from the table, the rise in R_ct and decrease in C_dl by utilizing the coating, especially with Thiourea, testify to forming a strong protective film

that reduces electrochemical reactions. The double-layer system at 25°C works best with R_ct being 1450 Ω cm^2 and C_dl decreasing to 42 μF/cm^2. Upon heating to 60°C, the values decrease significantly, with the loss of thermal stability, even though the double-layer system remains the best compared to the other conditions.

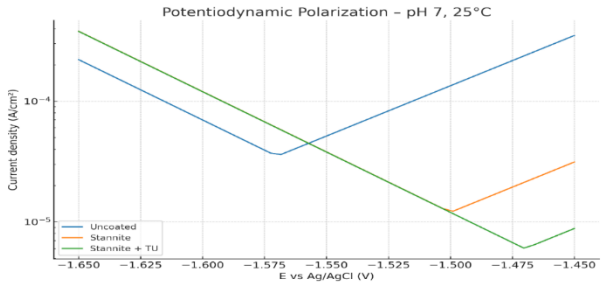


Fig. 10. Nyquist plots obtained from EIS measurements for uncoated, stannite-coated, and stannite-coated AZ91C specimens with thiourea (0.05 g/L) at pH 7 and 25°C in 3.5% NaCl solution.

Nyquist plots obtained from EIS measurements for uncoated, stannite-coated, and stannite-coated AZ91C specimens with thiourea (0.05 g/L) at pH 7 and 25°C in 3.5% NaCl solution. The larger semicircle diameters for coated and inhibitor-treated samples correspond to higher charge transfer resistance (R_ct), reflecting improved corrosion resistance and reduced electrochemical activity.

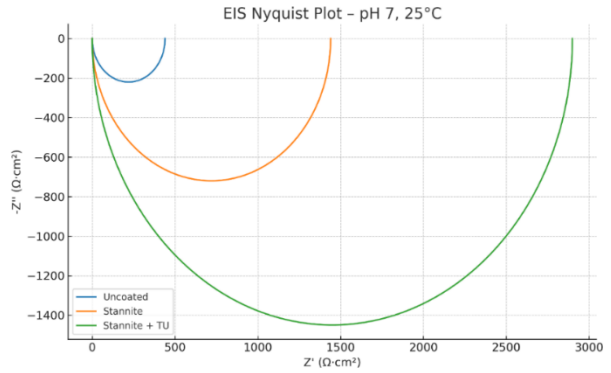


Fig. 11. Protection efficiencies for stannite coating (CE%), thiourea inhibitor (IE%), and the combined coating–inhibitor system (BE%) for AZ91C magnesium alloy at pH 7 and 25°C in 3.5% NaCl solution.

Protection efficiencies for stannite coating (CE%), thiourea inhibitor (IE%), and the combined coating–inhibitor system (BE%) for AZ91C magnesium alloy at pH 7 and 25°C in 3.5% NaCl solution. The combined system achieves the highest protection efficiency, demonstrating the synergistic effect of coating and inhibitor.

4.5 Mechanistic Interpretation

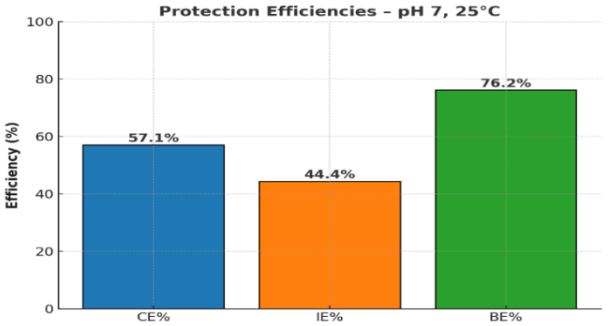


Fig. 12. SEM/EDS micrographs of stannite-coated AZ91C magnesium alloy surface morphology and elemental distribution after 48 h immersion at pH 7 and 25°C in 3.5% NaCl solution.

The figure shows the protection efficiency of AZ91C alloy at pH = 7 and 25 °C under three conditions: coating only (CE%) at 57.1%, inhibitor only (IE%) at 44.4%, and the combined system (BE%) at 76.2%. This indicates that combining the stannite coating with thiourea provides a significant synergistic effect, delivering the highest level of protection compared to using either method alone.

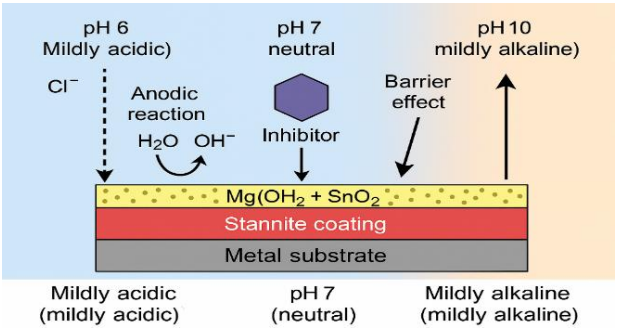


Fig. 13. Schematic representation of the synergistic protection mechanisms of AZ91C magnesium alloy with stannite coating and organic inhibitors under different pH conditions.

The figure shows that a magnesium alloy with stannite coating and an organic inhibitor such as thiourea provides good protection under various pH and temperature conditions. In neutral conditions, there is strong adsorption of the inhibitor; in acidic conditions, partial dissolution of the coating; and in alkaline conditions, a porous layer forms at high temperatures. This study is the first to compare the combined performance of the inhibitor and the coating using a multifactor ANOVA method. Stannite–TU possessed more than 76% protection efficiency at optimal conditions, comparable with other

established commercial protection systems such as phosphate systems with cerium inhibitors or organ silane systems. The ease of coating preparation, low inhibitor price, and high efficiency make the system ideal for industrial applications in the marine and automotive industries, which must withstand continuously changing environments. Standard testing (ASTM G31) also revealed that the efficiency was still over 65% even under extreme conditions (pH 6 at 60°C) and over 75% under moderate conditions, demonstrating the system's reliability.

Table 5. Efficiencies (CE%, IE%, BE%) of AZ91C Alloy under Different pH and Temperature Conditions (ASTM G31).

pH	T (°C)	CE%	IE%	BE%
6	25	55.2	38.5	72.4
6	40	42.2	46.2	68.9
6	60	42.3	42.2	66.7
7	25	57.1	44.4	76.2
7	40	46.9	47.1	71.9
7	60	45.8	43.8	69.5
10	25	46.7	37.5	66.7
10	40	40.9	46.2	68.2
10	60	36.8	45.8	65.8

The table shows the stannite–thiourea system protection efficiency (CE%), inhibitory efficiency (IE%), and overall efficiency (BE%) at various pH and temperatures. The efficiency is maximum at neutral pH (7) and low temperature (25°C), with a BE% of 76.2%. The efficiency continuously reduces with increasing temperature or in alkaline and acidic media, with the minimum value of 65.8% at pH 10 and 60°C. Still, overall efficiency remains above 65% in all the cases, indicating that the system effectively operates even in extreme conditions.

5. CONCLUSIONS

This study systematically evaluated the combined effects of pH and temperature on the corrosion behavior of AZ91C magnesium alloy in chloride solutions, with and without stannite conversion coatings and organic inhibitors (thiourea, benzotriazole, or sodium molybdate). Based on immersion testing, electrochemical characterization, and surface/phase analysis, the following conclusions can be drawn:

1. pH and temperature are dominant factors influencing corrosion rate, with higher temperatures and acidic conditions significantly accelerating degradation in both coated and uncoated specimens.
2. Stannite conversion coatings substantially improved corrosion resistance, achieving coating efficiencies (CE%) above 70% under mild conditions, although performance declined under aggressive environments (pH 6, 60°C).
3. Organic inhibitors provided additional protection, with optimal concentrations (0.03–0.05 g/L) reducing corrosion current density and increasing charge transfer resistance. TU performed best in neutral and mildly acidic conditions, while BTA exhibited superior performance in alkaline media.
4. Synergistic coating–inhibitor effects yielded combined efficiencies (BE%) exceeding 76% under optimal environmental conditions.
5. Surface and phase examination verified that the damage protection mechanisms include barrier coating development, inhibitor adsorption, and localized corrosion suppression.
6. The results provide valuable recommendations on reducing corrosion in AZ91C magnesium alloys subjected to marine and industrial conditions, based on which to select materials and design protection systems.

6. RECOMMENDATIONS

AZ91C alloy should be coated with stannite with thiourea inhibitor (0.05 g/L) in various applications. It finds application in contact systems in the marine industry, where it is found to have a neutral efficiency of more than 76%. It has been applied in the automotive sector in engine casing and body panels exposed to salt and moisture. It is suitable in aviation for non-critical applications since it is corrosion-resistant and lightweight, reducing maintenance. It is used in industrial machinery if exposed to detergents or corrosive environments at moderate temperatures. Thiourea is suitable in neutral and slightly acidic conditions, and benzotriazole is suitable in alkaline environments. A topcoat, such as a polymer coating, is recommended in severe environments to lengthen the life.

REFERENCES

[1] J. Su, W. L. Ng, J. An, W. Y. Yeong, C. K. Chua, and S. L. Sing, "Achieving sustainability by additive manufacturing: a state-of-the-art review and perspectives," *Virtual and Physical Prototyping*, vol. 19, no. 1, Dec. 2024, doi: 10.1080/17452759.2024.2438899.

[2] A. R. Santhi and P. Muthuswamy, "Industry 5.0 or industry 4.0S? Introduction to industry 4.0 and a peek into the prospective industry 5.0 technologies," *International Journal on Interactive Design and Manufacturing (IJIDeM)*, vol. 17, no. 2, pp. 947–979, Feb. 2023, doi: 10.1007/s12008-023-01217-8.

[3] R. V. Marode, T. A. Lemma, N. Sallih, S. R. Pedapati, M. Awang, and A. Hassan, "Research progress in friction stir processing of magnesium alloys and their metal matrix surface composites: Evolution in the 21st century," *Journal of Magnesium and Alloys*, vol. 12, no. 6, pp. 2091–2146, Jun. 2024, doi: 10.1016/j.jma.2024.06.007.

[4] M. S. R. Saleh, M. E. M. El-Garoshi, A. F. A. Fadiel, and H. M. B. Khalid, "The corrosion inhibition effect on the aluminum alloy AZ91C'S fatigue behavior in the saline environment," *European Journal of Materials Science and Engineering*, vol. 9, no. 1, pp. 19–28, Mar. 2024, doi: 10.36868/ejmse.2024.09.01.019.

[5] Y. Liu and X. Liu, "A study of Early-Stage corrosion behavior of AZ91 alloy and MAO-Coated alloy in 3.5% NACL solutions," *Materials*, vol. 15, no. 22, p. 7909, Nov. 2022, doi: 10.3390/ma15227909.

[6] M. S. Saleh, A. F. A. Fadiel, and H. M. Khalida, "Corrosion rate study of AZ91C magnesium alloy in sodium chloride solution of different concentrations using immersion method for coated and uncoated samples," *International Journal of Advances in Engineering Research*, vol. 26, 2023.

[7] A. Ortiz-Ozuna, M. Montoya-Rangel, H. Castaneda, F. A. Godínez, and R. Montoya, "Corrosion modeling of Magnesium and its alloys: A short review," *Materials Today Communications*, vol. 46, p. 112491, Apr. 2025, doi: 10.1016/j.mtcomm.2025.112491.

[8] L L. Ma *et al.*, "Dual-action self-healing protective coatings with photothermal responsive corrosion inhibitor nanocontainers," *Chemical Engineering Journal*, vol. 404, p. 127118, Sep. 2020, doi: 10.1016/j.cej.2020.127118.

[9] A. N. Singh, S. K. Swain, A. Meena, M. Islam, and K.-W. Nam, "Advances in Corrosion of High-Temperature Materials: Interfacial migration and alloy design strategies," *Ceramics*, vol. 7, no. 4, pp. 1928–1963, Dec. 2024, doi: 10.3390/ceramics7040121.

[10] D. Wan *et al.*, "Improving the corrosion resistance of AZ91 magnesium alloy by surface coating TIO2 layers," *Metals*, vol. 13, no. 8, p. 1400, Aug. 2023, doi: 10.3390/met13081400.

[11] J. Wasserbauer, M. Buchtík, J. Tkacz, S. Fintová, J. Minda, and L. Doskočil, "Improvement of AZ91 alloy corrosion properties by duplex NI-P coating deposition," *Materials*, vol. 13, no. 6, p. 1357, Mar. 2020, doi: 10.3390/ma13061357.

[12] T. Wu and K. Zhang, "Corrosion and protection of magnesium alloys: recent advances and future perspectives," *Coatings*, vol. 13, no. 9, p. 1533, Sep. 2023, doi: 10.3390/coatings13091533.

[13] J. Gou, M. Sun, X. Ma, G. Tang, and Y. Zhang, "Effects of temperature and pH value on the morphology and corrosion resistance of titanium-containing conversion coating," *Applied Surface Science Advances*, vol. 3, p. 100060, Jan. 2021, doi: 10.1016/j.apsadv.2021.100060.

[14] S. H. Jung and J.-H. Lee, "Corrosion behavior analysis of novel SN-2.5Ag-1.0Bi-0.8CU-0.05NI and SN-1.8Bi-0.75CU-0.065NI PB-Free solder alloys via Potentiodynamic Polarization Test," *Metals*, vol. 15, no. 6, p. 670, Jun. 2025, doi: 10.3390/met15060670.

[15] M. E. M. El-Garoshi, F. M. Hossen, A. F. A. Fadiel, and H. M. Khalid, "Investigation of corrosion resistance of magnesium alloy AZ91 immersed in sodium chloride solution at various concentrations utilizing the linear polarization method," *Middle European Scientific Bulletin*, vol. 41, no. 2, Oct. 2023, p. 5, doi: 10.47494/mesb.2023.41.

[16] V. Marakini, C. P, S. P. P, B. P. Achar, B. Sahoo, and U. Bhat, "Cryogenic machining induced corrosion resistance of magnesium alloy AZ91," *Next Materials*, vol. 8, p. 100600, Mar. 2025, doi: 10.1016/j.nxmate.2025.100600.

[17] Y. Li *et al.*, "Recent advances of high strength Mg-RE alloys: Alloy development, forming and application," *Journal of Materials Research and Technology*, vol. 26, pp. 2919–2940, Aug. 2023, doi: 10.1016/j.jmrt.2023.08.055.

[18] D.-I. Răuță, E. Matei, and S.-M. Avramescu, "Recent development of corrosion inhibitors: types, mechanisms, electrochemical behavior, efficiency, and environmental impact," *Technologies*, vol. 13, no. 3, p. 103, Mar. 2025, doi: 10.3390/technologies13030103.

[19] J. K. Balangao, "Corrosion of Metals: factors, types and prevention Strategies," *HAL (Le Centre Pour La Communication Scientifique Directe)*, Jan. 2024, [Online]. Available: https://hal.science/hal-04372559

[20] B. E. Ibrahimi, L. Guo, J. V. Nardeli, and R. Oukhrib, "The Application of Chitosan-Based Compounds against Metallic Corrosion," in *IntechOpen eBooks*, 2021. doi: 10.5772/intechopen.96046.

[21] A. Kadhim, A. Al-Amiery, Alazawi, M. Al-Ghezi, and R. Abass, "Corrosion inhibitors. A review," *International Journal of Corrosion and Scale Inhibition*, vol. 10, no. 1, Mar. 2021, doi: 10.17675/2305-6894-2021-10-1-3.

[22] N. T. Chung, Y.-S. So, W.-C. Kim, and J.-G. Kim, "Evaluation of the influence of the combination of pH, chloride, and sulfate on the corrosion behavior of pipeline steel in soil using response surface methodology," *Materials*, vol. 14, no. 21, p. 6596, Nov. 2021, doi: 10.3390/ma14216596.

[23] P. Kumari and M. Lavanya, "Optimization Strategies for Corrosion Management in Industries with Artificial Neural Network and Response Surface Technology: A Comprehensive Review," *Journal of Bio- and Tribo-Corrosion*, vol. 10, no. 3, Jun. 2024, doi: 10.1007/s40735-024-00863-z.

[24] F. Z. Akbarzadeh, E. R. Ghomi, and S. Ramakrishna, "Improving the corrosion behavior of magnesium alloys with a focus on AZ91 Mg alloy intended for biomedical application by microstructure modification and coating," *Proceedings of the Institution of Mechanical Engineers Part H Journal of Engineering in Medicine*, vol. 236, no. 8, pp. 1188–1208, Jun. 2022, doi: 10.1177/09544119221105705.

[25] M. M. Alves, C. Santos, and M. F. Montemor, "Improved corrosion resistance on Mg-2Ca alloy with TiO2 nanoparticles embedded in a polycaprolactone (PCL) coating," *Applied Surface Science Advances*, vol. 9, p. 100257, Apr. 2022, doi: 10.1016/j.apsadv.2022.100257.

[26] N. Y. Dudareva, M. M. Abramova, and R. V. Kalschikov, "Corrosion-Resistance of MAO-Coatings on Al-Si alloys," *Materials Science Forum*, vol. 870, pp. 83–89, Sep. 2016, doi: 10.4028/www.scientific.net/msf.870.83.

[27] Y. Li *et al.*, "Effects of duty cycle on properties of Ni–P–Al2O3 nanocomposite deposited layer prepared by pulse-assisted jet electrochemical deposition," *Journal of Materials Research and Technology*, vol. 21, pp. 3556–3569, Nov. 2022, doi: 10.1016/j.jmrt.2022.10.163.

[28] H. M. Khalid, A. F. A. Fadiel, M. S. Saleh, and M. E. El-Garoshi, "Effect of parameters on the electroplating of Ni–Co alloys in an ammonium citrate bath on yellow brass (C27200)," *Genius Repository*, vol. 23, pp. 43–51, 2023.

[29] K. Zhou *et al.*, "A view of magnesium alloy modification and its application in orthopedic implants," *Journal of Materials Research and Technology*, vol. 36, pp. 1536–1561, Mar. 2025, doi: 10.1016/j.jmrt.2025.03.188.

[30] L. P. Babu and R. Radha, "Advancements in magnesium-based alloys for orthopedic implants: balancing corrosion, mechanical properties, and biological effects (part 1) – a review," *Canadian Metallurgical Quarterly*, vol. 64, no. 4, pp. 2039–2064, Nov. 2024, doi: 10.1080/00084433.2024.2427455.

[31] L. M. Calado, M. J. Carmezim, and M. F. Montemor, "Rare Earth Based Magnesium Alloys—A review on WE Series," *Frontiers in Materials*, vol. 8, Jan. 2022, doi: 10.3389/fmats.2021.804906.

[32] W. Eljaafari, "Grain Refinement of AZ91 Mg-Ca-S Alloy (Review Paper)," *International Journal of Materials Technology and Innovation*, vol. 3, no. 1, pp. 90-95, Jan. 2023, doi: 10.21608/ijmti.2023.178821.1070.